# Dalton Transactions

Accepted Manuscript






ROYAL SOCIETY OF CHEMISTRY

www.rsc.org/dalton

# Light-induced spin-state switching in the mixed crystal series of the 2D coordination network $\{[Zn_{1-x}Fe_x(bbtr)_3](BF_4)_2\}_\infty$: optical spectroscopy and cooperative effects[#,‡]

Pradip Chakraborty,[1] Cristian Enachescu,[2] Arnaud Humair,[1] Leo Egger,[1] Teresa Delgado,[1] Antoine Tissot,[1] Laure Guénée,[3] Céline Besnard,[3]* Robert Bronisz,[4] and Andreas Hauser[1]*

[1]*Département de chimie physique, Université de Genève, 30 Quai Ernest-Ansermet, 1211 Genève, Switzerland*

[2]*Faculty of Physics, Al. I. Cuza University, 700506 Iasi, Romania*

[3]*Laboratoire de crystallographie, Université de Genève, 24 Quai Ernest-Ansermet, 1211 Genève, Switzerland*

[4]*Faculty of Chemistry, University of Wroclaw, F. Joliot-Curie 14, 50-383 Wroclaw Poland*

[#]Dedicated to Philipp Gütlich on the occasion of his 80th birthday

**Abstract**

Depending on the iron(II) concentration, the mixed crystals of $\{[Zn_{1-x}Fe_x(bbtr)_3](BF_4)_2\}_\infty$, bbtr = 1,4-di(1,2,3-triazol-1-yl)butane, $0.01 \leq x \leq 1$, show macroscopic light-induced bistability between the high-spin and the low-spin state. In the highly diluted system with $x = 0.01$ and up to $x = 0.31$, the photoinduced low-spin state always relaxes back to the high-spin state independent of the initial light-induced low-spin fraction. In the highly concentrated mixed crystals with $x = 0.67$, 0.87 and 1, the strong cooperative effects coupled to a crystallographic phase transition result in light-induced bistability with decreasing critical light-induced low-spin fraction and increasing hysteresis width for increasing iron(II) concentrations. The lower limit for the light-induced bistability is estimated at $x \approx 0.5$.

---

[‡]Electronic Supplementary Information (ESI) available. For ESI see DOI: xxx

## 1. Introduction

Spin-crossover complexes of transition metal ions with $d^4$-$d^7$ electronic configurations have become very topical.[1,2,3] Indeed, a large number of studies have been dedicated to this research field in the past years, focusing on their labile electronic nature as function of external stimuli such as pressure,[4,5] magnetic fields,[6,7] chemical variation,[8] temperature[9,10] and light.[9] Among these, it is well known that light can modify the population between high-spin (HS) and low-spin (LS) states of a given spin-crossover complex. In particular for iron(II) spin-crossover systems a long-lived metastable HS ($^5T_2$, $S = 2$) state can often be created from the LS ($^1A_1$, $S = 0$) ground state by wavelength-selective optical perturbation below the thermal spin transition temperature of a given complex,[9] a phenomenon known under the acronym of LIESST (Light-induced Excited Spin State Trapping). For some iron(II) spin-crossover systems, the reverse phenomenon, called reverse-LIESST, which involves the light-induced population transfer back to the LS state has also been observed.[9,11] Given the very different spectroscopic signatures for the electronic transitions of the two spin states in the UV-Vis-NIR regions, optical spectroscopy at variable temperatures is the method of choice for the investigation of the photophysical properties of such compounds. In particular, time-resolved single-crystal absorption spectroscopy allows the direct observation of relaxation processes over many orders of magnitude, that is, from the picosecond time regime for the initial relaxation processes among the higher excited states immediately following the excitation, to hours for the HS □ LS relaxation at low temperatures. Figure 1 summarises the light-induced processes in the case of iron(II) spin-crossover complexes with high-energy metal-ligand charge transfer (MLCT) states as for instance triazoles[12] and tetrazoles[11] based ligands, such that the low-energy ligand-field states can be clearly observed spectroscopically. Ultrafast pump-probe spectroscopy revealed that LIESST, either via irradiation into the $^1$MLCT transition[13] or spin-allowed ligand-field transitions[14], occurs with quantum efficiency of almost

unity, takes less than 1 ps, and without any indication of a population of an intermediate $^3$dd state. Reverse-LIESST on the other hand is only observed for irradiation into the spin-allowed $^5T_2 \rightarrow {}^5E$ ligand-field transition. Its overall quantum efficiency is low and it occurs as a two-step process, with the population of the intermediate state assigned to the $^3T_1$ state having a lifetime of around 40 ps at 120 K.[14]

In the solid-state, the difference in metal-ligand bond length of typically 0.2 Å between the HS and the LS state[15,16] generates elastic interactions between the spin active centres resulting in so-called cooperative effects, which strongly influence the thermal and light-induced spin-crossover phenomena.[17-26] The physics of elastic interactions and the corresponding cooperative phenomena are well established by means of theoretical models.[16,27-33] As light-induced spin-state switching has tremendous potential in the field of optical data storage[34] and display devices,[34,35] fundamental research, particularly focusing on the interplay between function and cooperative effects, is of current interest.

On lowering the temperature, the neat title compound, namely the 2D coordination network $\{[Fe(bbtr)_3](BF_4)_2\}_\infty$, bbtr = 1,4-di(1,2,3-triazol-1-yl)butane, stays in the HS ($^5T_2$) state down to 10 K.[18] This is in contrast to the perchlorate analogue, $\{[Fe(bbtr)_3](ClO_4)_2\}_\infty$, which is a spin-crossover compound showing an abrupt spin transition with a 13 K wide hysteresis centred at 107 K[36] as well as LIESST and reverse-LIESST at low temperatures.[12] It can, however, be switched to the LS ($^1A_1$) state by irradiation into the $^5T_2 \rightarrow {}^5E$ ligand-field transition in the NIR below 100 K.[37] Due to the above mentioned cooperative effects, the light-induced LS state is thought to correspond to a true minimum in the free energy below a certain temperature. The system can thus be regarded as a spin-crossover system showing a very large hysteresis with $T_c^{\uparrow}$ = 100 K and $T_c^{\downarrow}$ well below 50 K, that is, at a temperature where the LS HS relaxation is so slow that it never relaxes to the LS state. In order to understand the nature of the cooperative effects and the limit for the observation of such a light-induced

bistability, we herein discuss the wavelength-selective light-induced HS → LS switching behaviour as a function of iron(II) concentration in the series $\{[Zn_{1-x}Fe_x(bbtr)_3](BF_4)_2\}_\infty$, $0.01 \leq x \leq 1$. The detailed investigation of the light-induced spin-state switching and the relaxation processes will help us to understand the functional aspects of photoswitchable materials with respect to the variation of the fundamental elastic interactions in the solid state. The key features will be modelled based on a mean-field approach[33] in a comprehensive way also in comparison to the mixed crystal series of the corresponding perchlorate salt, namely the spin-crossover system $\{[Zn_{1-x}Fe_x(bbtr)_3](ClO_4)_2\}_\infty$.[18,39]

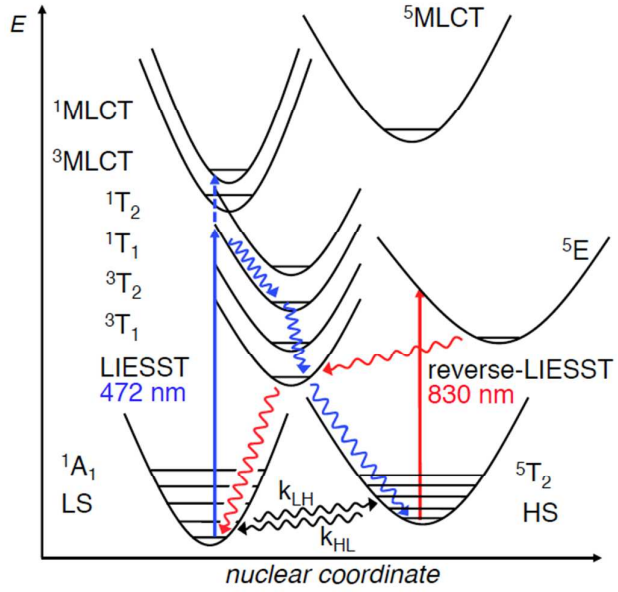


**Figure 1.** Schematic representation of the different electronic energy levels associated in the light-induced processes for $\{[Zn_{1-x}Fe_x(bbtr)_3](BF_4)_2\}_\infty$, LIESST for irradiation at 472 nm, reverse-LIESST for irradiation at 830 nm (adapted from refs 9 and 11]).

## 2. Experimental

High-quality mixed crystals of $\{[Zn_{1-x}Fe_x(bbtr)_3](BF_4)_2\}_\infty$, were grown as previously reported.[18, 36] They are hexagonal in shape, transparent and colourless at room temperature as well as at low temperature. Their average size varies between 100 and 150 μm and they cleave easily perpendicular to the crystallographic *c*-axis. The space group at $T$ = 295 K is $P\bar{3}$.[18] In

spin-crossover research, traditionally magnetic susceptibility measurements and Mössbauer spectroscopy are the most commonly employed experimental methods. However, for dynamic investigations their time window and for dilute mixed crystals their sensitivity is limited. Optical spectroscopy circumvents both problems as its dynamic range goes from picoseconds for ultrafast pump-probe methods to hours using conventional methods. Even though diffuse reflectance spectroscopy has been shown to be a useful tool in spin-crossover research,[38] we prefer single-crystal absorption spectroscopy as it allows a more quantitative evaluation of the data. To this effect crystals were mounted on pinholes with the *c*-axis perpendicular to the pinholes using thermal contact glue. The spectra were recorded on a double beam scanning spectrometer (Cary 5000) or a home-built system with non-polarised light propagating along the *c*-axis. Slow kinetic traces were determined on these set-ups by recording full spectra at given time intervals. Relaxation curves below 1 s down to tens of nanoseconds were recorded in transient absorption at single wavelengths using the home-built set-up. For continuous wave irradiation at 830 nm (reverse-LIESST) a laser diode (ILEE Model Z40KV1) and at 472 nm (LIESST) a diode pumped solid-state laser (ILEE VA-I-N-472) with typical intensities of a few $mW/mm^2$ were used. For time-resolved measurements down to the nanosecond time scale, excitation at 830 nm came either from the idler output of a MOPO (Optotek Magic Prism) pumped by the third harmonic of a Nd:YAG laser (Quantel Brillant) or at 532 nm directly from the second harmonic of the same laser. Variable temperatures down to 10 K were achieved with a closed cycle cryosystem (Janis-Sumitomo SHI-4-5) equipped with a computer controlled temperature controller. Further details of the experimental setups are given in refs 39 and 40.

For photo-crystallographic experiments crystals of approximately $150\times150\times20$ $\mu m^3$ were mounted on a kapton cryoloop with silicon grease. Diffraction data at low temperature (10K) in a helium open flow cryosystem (Oxford Diffraction Helijet) were collected at the Swiss Norwegian Beam Line (SNBL) BM01A at the European Synchrotron Radiation Facility

(ESRF), Grenoble, France (synchrotron radiation λ = 0.69412 Å), using a Pilatus2M pixel area detector from Dectris Ltd. For irradiation at 830 nm the above-mentioned laser diode was used. More details with regard to data collection and structure refinement are given in the Supporting Information.

## 3. Results and discussion

### 3.1. Reverse-LIESST and light-induced bistability

Figure 2 shows the high-quality single-crystal absorption spectra of the mixed-crystals of $\{[Zn_{1-x}Fe_x(bbtr)_3](BF_4)_2\}_\infty$, $x$ = 0.01, 0.31, 0.48, 0.67, 0.87 and 1. Each panel of Figure 2 contains the spectrum at room temperature, the spectrum at 10 K before irradiation after cooling down at a rate of 0.2 K/min (assignment of bands according to the red arrows in Figure 1), the spectrum at 10 K after irradiation at 830 nm (assignments according to blue arrows in Figure 1), and the series of spectra as a function of temperature while heating from 10 K at a constant rate of 0.2 K/min after irradiation. Depending on the dilution, the evolution of either the intense $^1$MLCT band centred at 320 nm (31250 cm$^{-1}$) with ε ≈ 10000 M$^{-1}$cm$^{-1}$ (for $x$ = 0.01) or the weaker $^1A_1 \rightarrow {}^1T_1$ ligand-field band centred at 547 nm (18280 cm$^{-1}$) with ε = 28 M$^{-1}$cm$^{-1}$ (for $x$ = 0.31, 0.48, 0.67, 0.87 and 1) is followed in order to monitor the changes in the population of the spin-states. This is due to the fact that for highly diluted mixed-crystals such as $x$ = 0.01, the intensity of $^1$dd bands is too weak to be observed, whereas for the concentrated mixed-crystals, the intensity of the $^1$MLCT is too intense such that it becomes saturated. The spectra at room temperature and upon cooling to 10 K are almost superimposable, which indicates that the complexes stay in the HS state down to that temperature. After irradiation at 830 nm (12050 cm$^{-1}$), that is, irradiation into the even weaker $^5T_2 \rightarrow {}^5E$ ligand-field band with ε = 5 M$^{-1}$cm$^{-1}$ centred at that wavelength and just discernible in the spectrum for $x$ = 1, the characteristic $^1$MLCT band (for $x$ = 0.01) at 320 nm or the $^1A_1 \rightarrow {}^1T_1$ and $^1A_1 \rightarrow {}^1T_2$ bands (for $x$ = 0.31, 0.48, 0.67, 0.87 and 1) at 547 and 380 nm respectively appear via reverse-LIESST.

Prolonged irradiation at 830 nm results in a steady state population $\gamma_{LS}^{ss}$ of 85% in the LS state due to the spectral overlap between the spin-allowed and the spin-forbidden bands of the HS and the LS species, respectively.[9,11]

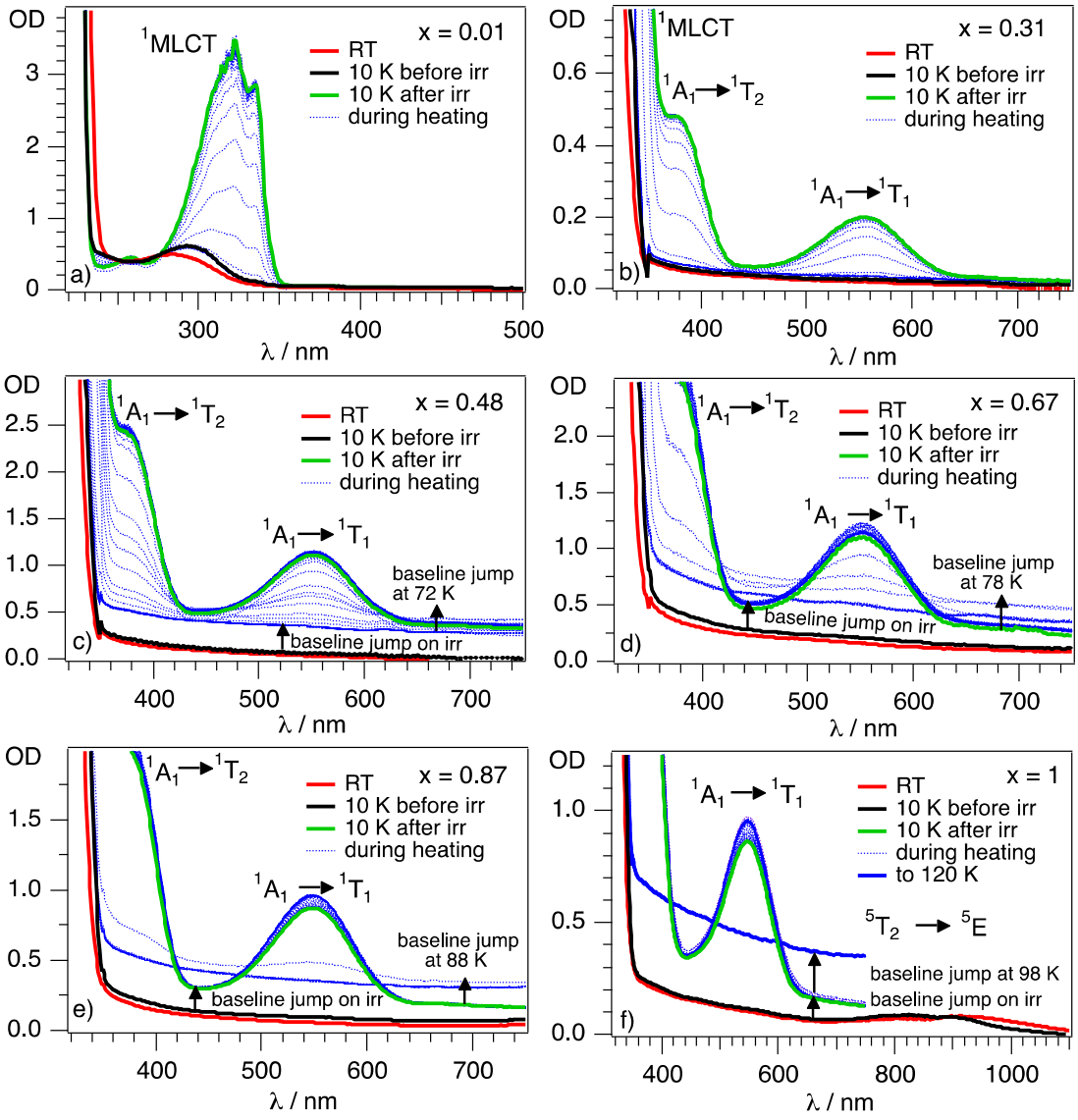


**Figure 2.** High-quality single-crystal absorption spectra of $\{[Zn_{1-x}Fe_x(bbtr)_3](BF_4)_2\}_\infty$, for a) $x = 0.01$, b) $x = 0.31$, c) $x = 0.48$, d) $x = 0.67$, a) $x = 0.87$, and f) $x = 1$, d = 60 – 100 μm. Each panel shows the spectrum at room temperature (red), the spectrum at 10 K before irradiation (black), the spectrum at 10 K after irradiation at 830 nm, 10 mW/mm$^2$ (green), and intermediate spectra at different temperatures during heating at a rate of 0.2 K/min (blue dotted lines).

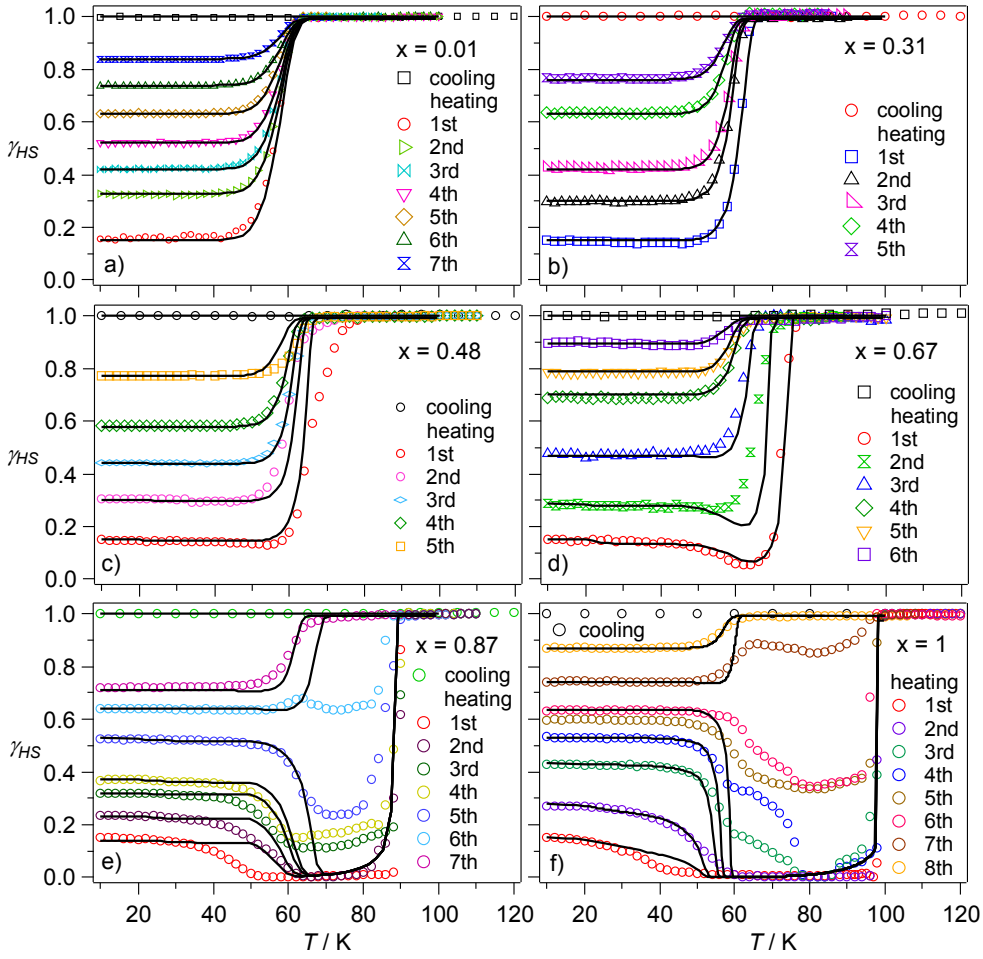


**Figure 3.** Evolution of the HS fraction, $\gamma_{HS}$, as a function of temperature after partial photoexcitation to the LS state by irradiation at $\lambda_{ex}$ = 830 nm (10 mW/mm$^2$) at 10 K for $\{[Zn_{1-x}Fe_x(bbtr)_3](BF_4)_2\}_\infty$, with a) $x$ = 0.01, b) $x$ = 0.31, c) $x$ = 0.48, d) $x$ = 0.67, e) $x$ = 0.87, and f) $x$ = 1. The heating rate is 0.2 K/min. Numerically calculated curves using the mean-field approximation according to equation (3) with $\Delta H^0_{HL}$ = 395 K, $\Delta S^0_{HL}$ = 5 and $\Gamma = \Delta_M$ = 380 K (—), the values for $k^0_{HL}(x \to 0, T)$ at every temperature were taken from Figure 7.

During heating in the dark with a sweep rate of 0.2 K/min after first creating the 85% steady state LS population, the intensities of the $^1$MLCT or $^1$dd bands (dotted blue spectra in Figure 2) change as a function of temperature. Accordingly, Figure 3 shows the evolution of the HS fraction, $\gamma_{HS}$, monitored from the variation of the spectral intensity as a function of temperature for $\{[Zn_{1-x}Fe_x(bbtr)_3](BF_4)_2\}_\infty$, for x = 0.01, 0.31, 0.48, 0.67, 0.87 and 1. For the more

concentrated mixed-crystals, that is with $x \geq 0.48$, the spectra show a first jump of the baseline during irradiation and a second jump at different temperatures during heating. Such baseline jumps are attributed to an increase in diffuse scattering due to the domain structure resulting from a crystallographic phase transition.[12] Thus in analogy to the neat compound, for higher iron(II) concentrations, the light-induced HS→LS conversion triggers the crystallographic phase transition from $P\bar{3}$ to $P\bar{1}$ resulting in the first baseline jump. On heating, the second baseline jump occurs at the temperature where the system returns to the $P\bar{3}$ phase and at the same time to the HS state.

Figure 3 includes curves obtained in the same way following partial photo-induced LS fractions created by varying the irradiation time. For all concentrations during the heating at a constant rate of 0.2 K/min, no changes are observed up to around 50 K for all initial concentrations due to the slow spin-state relaxation dynamics below that temperature. Above 50 K, the relaxation dynamics become faster, and depending upon the iron(II) concentration in the mixed-crystals and the initial photo-induced LS population, different relaxation behaviours are observed: (i) In the highly diluted mixed system with $x$ = 0.01 (Figure 3a), the photo-induced LS population simply returns to the HS state. As in the highly diluted systems the cooperative effects are absent, individual iron(II) centres relax independently of each other, and therefore the temperature at which half of the converted complexes have returned to the HS state, $T_{r\text{-}LIESST}$ = 57 K, does not depend on the initial light-induced LS fraction. (ii) For the mixed-crystals with $x$ = 0.31 and 0.48 (Figures 3b and c), a similar behaviour is observed, except that the temperature at which the population returns to the HS state moves to slightly higher temperatures with increasing initial LS fraction and increasing value of $x$. This variation of $T_{r\text{-}LIESST}$, displayed in Figure 4a, is attributed to the cooperative effects, which begin to manifest themselves already for the quite low iron(II) concentrations. (iii) For the mixed system with $x$ = 0.67 (Figure 3d) the photo-induced LS population also relaxes back to the HS

state, but the dependence of $T_{r\text{-}LIESST}$ on the initial LS population is stronger. Additionally, at this iron(II) concentration, for the light-induced steady-state LS population $\gamma_{LS}^{ss}$ of 85%, the complexes first relax further towards the LS state between 50 and 65 K, before again returning to the HS state above 65 K. This is now definitely due to moderately strong cooperative effects at this value of $x$. (iv) For the concentrated mixed crystals with $x$ = 0.87 and 1 (Figures 3e and f) the relaxation depends even more strongly on the initial light-induced LS fraction. Firstly, for very small initial LS populations, the relaxation still goes directly to the HS state at the same temperature as for the more dilute systems. Secondly, the shift towards higher temperature with increasing initial LS fraction is more pronounced. Thirdly, if the initial photo-induced LS population is higher than approximately 45% for $x$ = 0.87 and 35% for $x$ = 1, the relaxation first goes towards an increasing LS population, reaching the full LS state for high enough initial LS fractions. This indicates that in the highly concentrated and neat compound, the strong cooperative effects of elastic origin result in a light-induced bistability.[37,40-46] Fourthly, for these higher initial LS fractions the return to the HS state is very abrupt, occurs at 88 and 100 K for $x$ = 0.87 and 1, respectively, does not depend on the initial LS fraction and coincides with the jump in the baseline of the absorption spectra due to the above mentioned crystallographic phase transition. This temperature is therefore not a dynamic relaxation temperature as expressed by $T_{r\text{-}LIESST}$ anymore, but rather the thermodynamic temperature of the phase transition in the heating direction $T_c^{\uparrow}$ as indicated by the jump in the corresponding curves shown in Figure 4a. And last but not least, for intermediate initial LS fractions the relaxation behaviour becomes more complex, with steps suggesting a superposition of different relaxation mechanisms.

Qualitatively, we can conclude that at low iron(II) concentrations, the HS state is the quantum mechanical ground state as well as the thermodynamically stable state at all temperatures. The light-induced LS state is but a kinetically trapped, metastable state and relaxes back to the HS

state at temperatures above 50 K. At higher iron(II) concentrations this is no longer necessarily the case. On the light-induced HS → LS conversion, at a certain light-induced LS fraction a crystallographic phase transition from $P\bar{3}$ to $P\bar{1}$ with a doubling of the unit cell along the *c*-axis is triggered,[37,40] in analogy to the symmetry lowering, but without the doubling, also observed during the thermal spin transition to the LS state in the cooling branch of the perchlorate analogues.[18,36] Above this critical light-induced LS fraction, $\gamma_{LS}^{crit}$, the LS state becomes the quantum mechanical ground state due to the cooperative effects, which tend to stabilise the majority species.[33] Therefore at temperatures where the LS□HS relaxation becomes appreciable, that is, above ~50 K, the remaining iron(II) centres also relax to the LS state. For an initial light-induced LS fraction below this critical value, the system relaxes to HS state.

The limits of the light-induced bistability, that is, the temperature, the iron(II) concentration and the critical light-induced LS population, at which the LS state becomes sufficiently stabilised to become the thermodynamically stable state, can be quantified. Figure 4a demonstrates the two regimes for the LS → HS relaxation, namely $T_{r\text{-}LIESST}$ as a function of the initial LS fraction for the different values of *x*, and $T_c^{\uparrow}$ for values of *x* and the initial LS fraction above the threshold values, which trigger the crystallographic phase transition. Figure 4b shows the values of $T_{r\text{-}LIESST}$ and $T_c^{\uparrow}$ for an initial LS fraction corresponding to the steady state fraction $\gamma_{LS}^{ss}$ of 85% on irradiation at 830 nm as a function of *x*. From the crossing point of the two lines corresponding to the two regimes in Figure 4b, a minimal iron(II) concentration of $x \approx 0.5$ seems to be required in order to trigger the phase transition at the maximum achievable light-induced LS population of 85%. These values coincide with the ones for the thermal spin transition of the perchlorate analogue, where for $x = 0.48$, the crystallographic $P\bar{1}$ to $P\bar{3}$ phase transition in the heating branch occurs for approximately $\gamma_{LS} = 0.8$ at $T_c^{\uparrow} = 83$ K.[39]

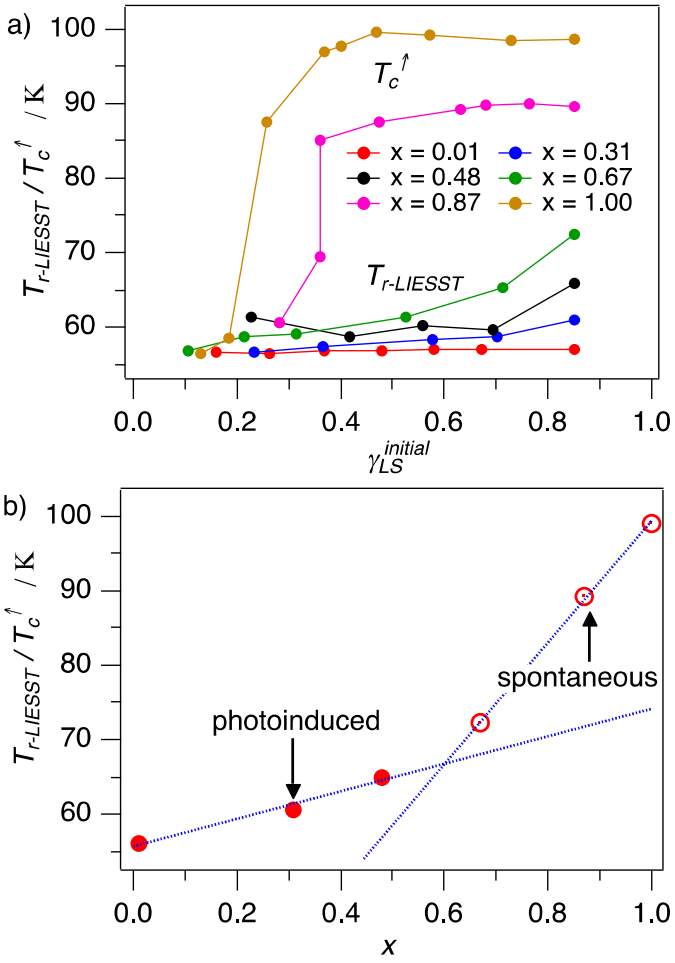


**Figure 4.** a) Variation of $T_{r\text{-}LIESST}$ as a function of the initially populated LS fraction $\gamma_{LS}^{initial}$ by varying the irradiation time for iron(II) concentrations and initial light-induced LS fractions which do not induce a crystallographic phase transition, and $T_c^{\uparrow}$ of the crystallographic phase transition for higher values of $x$ and $\gamma_{LS}^{initial}$. Irradiation was performed at 830 nm (10 mW/mm$^2$); b) Variation of $T_{r\text{-}LIESST}$ for $x$ < 0.5 (●) and of $T_c^{\uparrow}$ for $x$ > 0.5 (⊙) as a function of $x$ in $\{[Zn_{1-x}Fe_x(bbtr)_3](BF_4)_2\}_\infty$ for an initial light-induced LS fraction of 85%.

In the next step, the minimum value of $x$ has to be determined, for which light-induced bistability is observed. For low iron(II) concentrations, that is $x$ = 0.01 and 0.31, this is never the case, as exemplified by the relaxation curves shown in Figure 5a and b at different temperatures for the initial light-induced steady state LS fraction $\gamma_{LS}^{ss}$ of 85%, and in Figure 6 a

and b for different initial LS fractions at fixed temperatures. Whatever the conditions, above around 50 K only LS $\rightarrow$ HS relaxation is observed, even though for $x$ = 0.31, cooperative effects already are apparent in the sigmoidal shape of the relaxation curves for high values of the light-induced LS fraction. For these two values of $x$, the HS state is therefore always the thermodynamically stable state as already inferred from the temperature scan experiments. For $x$ = 0.48, the relaxation curves at different temperatures starting from a light-induced LS fraction of 85% (Figure 5c) show a very sluggish behaviour. For instance at 50 K, the system doesn't seem to be able to make up its mind in which direction to relax. Thus at this temperature and at a LS fraction of 85%, the Gibbs free energy difference between the two states must be very close to zero. For higher temperatures, the entropy gain wins and the relaxation goes towards the HS state. For $x$ = 0.67 the light-induced bistability becomes evident from the corresponding panels in Figures 5d and 6c. For this value of $x$, persistent switching can be achieved below 65 K and requires a critical light-induced LS fraction, $\gamma_{LS}^{crit}$, of 85% just below that temperature, and of about 70% at 55 K. The threshold value of $x$ for the occurrence of a light-induced bistability must therefore be between 0.48 and 0.67, but probably closer to 0.48 by interpolation.

For $x$ = 1, it's the other way round. For all temperatures below 100 K, the relaxation from the light-induced steady state LS fraction $\gamma_{LS}^{ss}$ of 0.85 results in a complete population of the LS state, and as can be inferred from Figure 6d, at 60 K a light-induced critical LS fraction $\gamma_{LS}^{crit}$ of only 30% is sufficient to result in relaxation to full LS population after switching off the irradiation and warming to above 50 K. The strongly sigmoidal shape underlines the importance of the cooperative effects. As previously discussed, $\gamma_{LS}^{crit}$ also depends on temperature.[40]

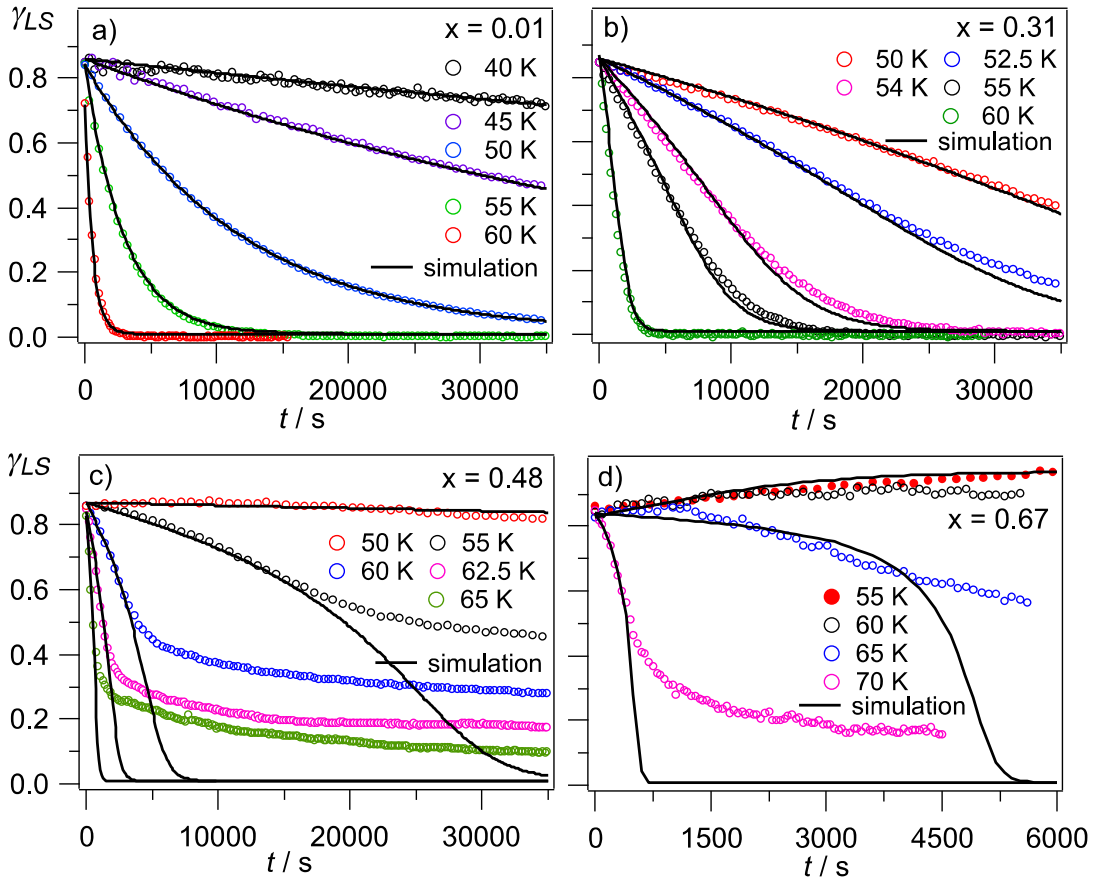


**Figure 5.** Photo-induced LS → HS relaxation curves at various temperatures as a function of time for $\{[Zn_{1-x}Fe_x(bbtr)_3](BF_4)_2\}_\infty$, a) $x$ = 0.01, b) $x$ = 0.31, c) $x$ = 0.48, d) $x$ = 0.67, after irradiation at 830 nm (10 mW/mm$^2$) to their steady-state value of $\gamma_{LS}$ = 0.85. Calculated relaxation curves in mean-field approximation with $\Delta H^0_{HL}$ = 395 K, $\Delta S^0_{HL}$ = 5 and $\Gamma = \Delta_M$ = 380 K (—).

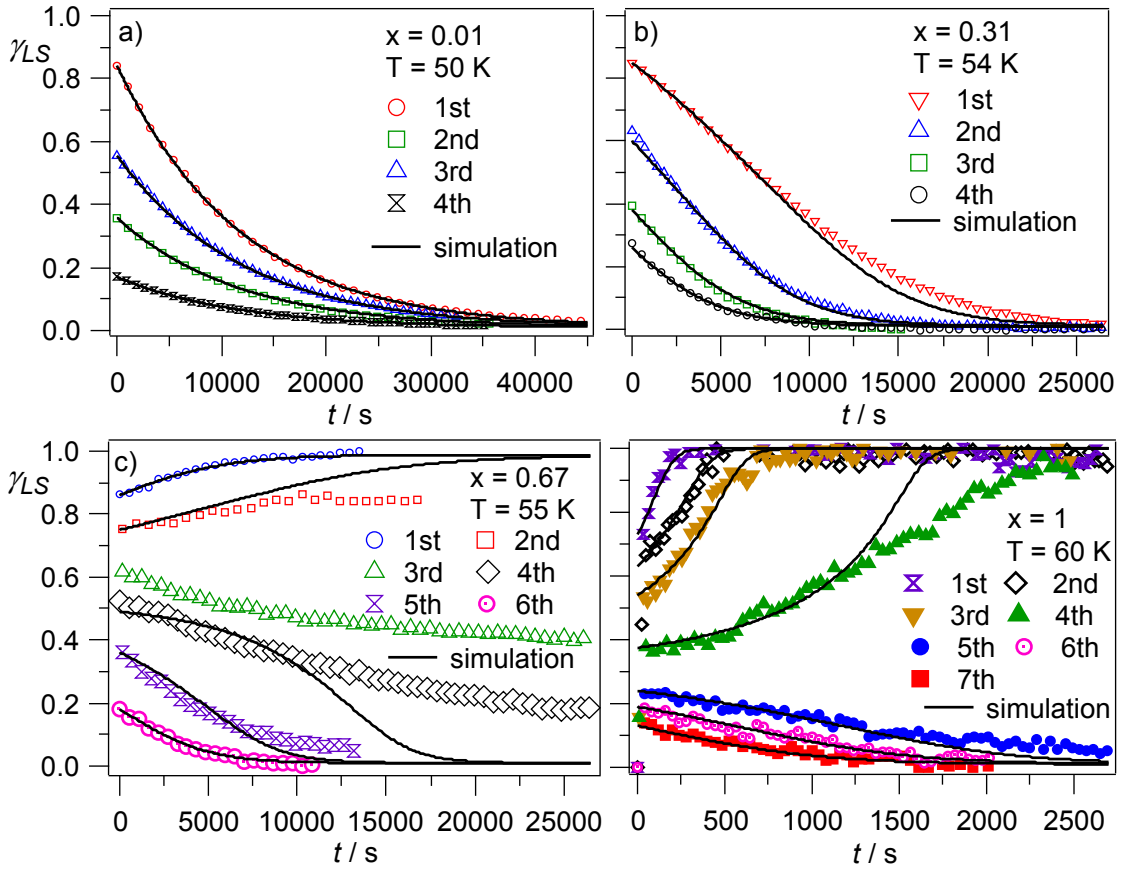


**Figure 6.** Photo-induced LS → HS relaxation curves for various light-induced initial LS fractions for $\{[Zn_{1-x}Fe_x(bbtr)_3](BF_4)_2\}_\infty$, a) $x$ = 0.01 at 50 K, b) $x$ = 0.31 at 54 K, c) $x$ = 0.67 at 55 K, and d) $x$ =1, after irradiation at 830 nm (10 mW/mm$^2$). Calculated relaxation curves in mean-field approximation with $\Delta H^0_{HL}$ = 395 K, $\Delta S^0_{HL}$ = 5 and $\Gamma = \Delta_M$ = 380 K (—).

In summary, the mixed crystal system, $\{[Zn_{1-x}Fe_x(bbtr)_3](BF_4)_2\}_\infty$, shows a light-induced persistent bistability for $x > 0.5$ below a given temperature, which depends on $x$. As shown in ref. 40, for the neat compound this is equivalent to saying $\{[Fe(bbtr)_3](BF_4)_2\}_\infty$ is a spin-crossover compound with a very wide hysteresis such that $T_c^{\uparrow}$ = 100 K and $T_c^{\downarrow}$ is below 30 K. The latter could even be formally negative. Dilution with Zn reduces the cooperative effects, thus the width of the hysteresis is reduced, and as is common for Zn as host, the transition temperature is lowered. Thus as observed, $T_c^{\uparrow}$ moves to lower temperatures with decreasing values of $x$, but $T_c^{\downarrow}$ remains elusive. In the region of bistability and at a temperature of

approximately 55 K, the critical value of the light-induced LS fraction increases with decreasing values of $x$ such that $x\gamma_{LS}^{crit} \approx 0.35 \approx$ constant. This indicates that the internal stress created by the smaller LS complexes triggers the crystallographic phase transition. Below $x \approx$ 0.4 the crystallographic phase transition is not observed anymore, and at the same time the light-induced bistability also disappears. It must therefore be concluded that the two are intimately linked. The comparatively complex relaxation behaviour shown in Figure 3 for high values of $x$ and intermediate values of the initial light-induced LS fraction is likewise due to the kinetics of the crystallographic phase transition, that is, to nucleation and growth phenomena.

### 3.2. X-ray crystallography and the crystallographic phase transition

As mentioned above, at room temperature $\{[Fe(bbtr)_3](BF_4)_2\}_\infty$ crystallises in the trigonal space group $P\bar{3}$ and stays in this space group down to 10 K on slow cooling without irradiation, that is, as long as it stays in the HS state.[18,40] The same holds for whole series of mixed crystals $\{[Zn_{1-x}Fe_x(bbtr)_3](BF_4)_2\}_\infty$ (see supporting information), in particular also for neat $\{[Zn(bbtr)_3](BF_4)_2\}_\infty$. In $P\bar{3}$ all metal centres are crystallographically equivalent and all metal-ligand bond lengths are the same. As described previously, the structure is a 2D polymeric network with the layers stacking along the c axis (see Figure S1 in Supporting Information). The corresponding cell parameters for different values of $x$ and the average metal-nitrogen bond lengths are given in Table 1. Assuming that the average metal ligand bond lengths as obtained from the single crystal data analysis of the mixed crystals are given by

$$\left\langle r_{M-N} \right\rangle = x r_{HS} + \left(1-x\right) r_{Zn-N} \qquad (1)$$

it is possible to extract the metal-ligand bond length of the iron(II) complex in the HS state for various values of $x$. These are included in Table 1. Within experimental accuracy, they are all equal to the value for the neat iron(II) compound.

Irradiating either the neat iron(II) compound or the mixed crystals at 10 K with light at 830 nm transforms the HS complexes to the LS state up to the steady state population of $\gamma_{LS}^{ss}$ = 0.85. For $x$ = 0.31, it is now also possible to determine the iron-nitrogen bond length in the LS state. For this iron(II) concentration, the system stays in the high-symmetry space group $P\bar{3}$ during and after the irradiation. The average metal-nitrogen bond length is therefore given by

$$\left\langle r_{M-N} \right\rangle = x\left(\gamma_{LS}^{ss} r_{LS} + \left(1-\gamma_{LS}^{ss}\right) r_{HS}\right) + \left(1-x\right) r_{Zn-N} \qquad (2)$$

The corresponding value of $r_{LS}$ is given in Table 1. With it $\Delta r_{HL} = r_{HS} - r_{LS}$ = 0.19 Å, that is, the difference in iron(II)-nitrogen bond length between the HS state and the light-induced LS state is in accordance with values found for thermal spin transition of the perchlorate analogue[18] and for the reverse LIESST structure of neat $\{[Fe(bbtr)_3](BF_4)_2\}_\infty$.[40] The latter had been determined by irradiating a crystal at 10 K to the steady state value $\gamma_{LS}^{ss}$ = 0.85, then heating the crystal to 65 K in order for the remaining HS fraction to relax to the LS state and finally re-cooling the sample to 10 K.[40]

As mentioned above, even for values of $x$ > 0.5, the trigonal space group is maintained during cooling to 10 K as long as the system stays in the HS state, but similar to the neat compound,[37,40] upon irradiation at a certain critical light-induced LS fraction assumed to be around a value such that $x\gamma_{LS}^{crit} \approx 0.35$, the crystallographic phase transition from $P\bar{3}$ to $P\bar{1}$, with a doubling of the unit cell along the c-axis occurs, but still all metal centres are crystallographically equivalent. As the crystallographic phase transition results in twinning, it is not straightforward to solve the structure and the quality of the structure is not as good as before irradiation. Nevertheless, for the neat iron(II) compound, a satisfactory structure refinement in the light-induced HS state could be achieved,[40] and an average structure in the trigonal unit-cell could be refined for x = 0.67 (see Supporting Information). Table 1 lists the average values of the metal-nitrogen bond lengths and $c/2$ and $V_c/2$ for $P\bar{1}$ in order to facilitate

direct comparison with the values for $P\bar{3}$. The LS iron(II)-nitrogen bond lengths for both $x = 1$ as well as for $x = 0.67$ calculated using equation (2) are within experimental accuracy equal and give a bond length difference of $\Delta r_{HL} = 0.19$ Å. Finally, for higher values of $x$ on heating to above the respective $T_c\uparrow$, the systems return to the high symmetry phase $P\bar{3}$.

**Table 1.** a) Unit cell parameters and metal-nitrogen bond lengths for $\{[Zn_{1-x}Fe_x(bbtr)_3](BF_4)_2\}_\infty$, $x = 0$, 0.31, 0.67 and 1. For all systems except for $x = 0.67$ and 1 after irradiation at 830 nm, the space group is $P\bar{3}$ (for more structural data see Supporting Information). b) For direct comparison values from the literature for $\{[Fe(bbtr)_3](BF_4)_2\}_\infty$, $\{[Zn(bbtr)_3](BF_4)_2\}_\infty$ and $\{[Zn(bbtr)_3](ClO_4)_2\}_\infty$ at 95 K, and $\{[Fe(bbtr)_3](ClO_4)_2\}_\infty$ in the HS and the LS state at ~100 K.

| a) T = 10 K | | $a$ [Å] | $c$ [Å] | $V_c$ [Å$^3$] | $\langle r_{M\text{-}N}\rangle$ [Å] | $r_{Fe\text{-}N}$ [Å] |
|---|---|---|---|---|---|---|
| $\{[Zn(bbtr)_3](BF_4)_2\}_\infty$ | | 11.587 | 7.543 | 877 | 2.170 | |
| $\{[Zn_{1-x}Fe_x(bbtr)_3](BF_4)_2\}_\infty$ | $\gamma_{HS} = 1$ | 11.591 | 7.537 | 877 | 2.180 | 2.202 |
| $x = 0.31$ | $\gamma_{LS} = 0.85$ | 11.530 | 7.578 | 872 | 2.130 | 2.012 |
| $\{[Zn_{1-x}Fe_x(bbtr)_3](BF_4)_2\}_\infty$ [a] | $\gamma_{HS} = 1$ | 11.594 | 7.536 | 877 | 2.182 | 2.185 |
| $x = 0.67$ | $\gamma_{LS} = 0.85$[a] | 11.455 | 7.602 | 864 | 2.080 | 1.978 |
| $\{[Fe(bbtr)_3](BF_4)_2\}_\infty$ [b] | $\gamma_{HS} = 1$ | 11.606 | 7.536 | 879 | 2.188 | 2.188 |
| | $\gamma_{LS} = 1$[a] | 11.309 | 7.621 | 849 | 1.993 | 1.993 |
| b) T = 90 – 100 K[b] | | | | | | |
| $\{[Fe(bbtr)_3](BF_4)_2\}_\infty$ | $\gamma_{HS} = 1$ | 11.621 | 7.553 | 883 | 2.190 | 2.190 |
| $\{[Zn(bbtr)_3](BF_4)_2\}_\infty$ | | 11.608 | 7.558 | 882 | 2.170 | |
| $\{[Fe(bbtr)_3](ClO_4)_2\}_\infty$ | $\gamma_{HS} = 1$ [c] | 11.601 | 7.717 | 901 | 2.193 | 2.193 |
| | $\gamma_{LS} = 1$[d] | 11.367 | 7.846 | 876 | 1.999 | 1.999 |
| $\{[Zn(bbtr)_3](ClO_4)_2\}_\infty$ [d] | | 11.621 | 7.704 | 898 | 2.168 | |

[a] average structure refined in $P\bar{3}$, [b] from ref 40 , refined in $P\bar{1}$ with doubling of c-axis, bond lengths correspond to average values, average value of $a$ and $b$, $c/2$ and $V_c/2$; [c] from ref. 18 refined in $P\bar{3}$ for $\gamma_{HS} = 1$, [d] from ref. 18, refined in $P\bar{1}$ for $\gamma_{LS} = 1$, average values of $a$ and $b$, and bond lengths.

Table 1 also lists selected structural parameters of the title system at around 100 K together with those of the perchlorate analogues form ref. 18. Compared to the perchlorate, the smaller $BF_4^-$ anions result in denser packing along the *c*-axis, thus pulling the layers of the 2D network closer to each other. On the other hand, the *a*-axis is systematically longer, indicating that as the $BF_4^-$ anions penetrate more deeply into the voids in the hexagonal sheets, the network is stretched a little in the *a/b* plane. This may be the reason for the slightly smaller ligand-field strength leading to a stabilisation of the HS state and the larger hysteresis of the spin transition.

### 3.3. Model calculations

Obviously, with a crystallographic phase transition involved, modelling the spin transition behaviour is not straightforward. As a first approximation, within a given phase, we will account for the experimental data with the master equation based on the mean-field approximation for the cooperative effects

$$\frac{d\gamma_{HS}}{dT} = -\frac{d\gamma_{LS}}{dT} = -k_{HL}^{0}\left(x,T\right)\exp\left(\frac{\Gamma x\left(1-\gamma_{HS}\right)}{k_B T}\right)\gamma_{HS} + k_{HL}^{0}\left(x,T\right)\exp\left(\frac{\Gamma x\left(1-\gamma_{HS}\right)}{k_B T}\right)\exp\left(-\frac{\Delta H_{HL}^{0} - T\Delta S_{HL}^{0} - 2\Gamma x\left(\gamma_{HS}-1/2\right) - \Delta_M\left(1-x\right)}{k_B T}\right)\left(1-\gamma_{HS}\right) \quad (3)$$

which includes both HS→LS and LS→HS relaxation processes.[39] In equation (3) $\Delta H_{HL}^{0}$ and $\Delta S_{HL}^{0}$ are the standard enthalpy and entropy variations for the pure compound, $k_{HL}^{0}$ is the HS→LS relaxation rate constant at $\gamma_{HS} = 1$, $\Gamma$ is the interaction parameter, and $\Delta_M$ accounts for a correction to the enthalpy difference of the spin change for diluted systems. As the zinc(II) structure is quite close to the iron(II) structure in the HS state, the lattice parameter $\Delta_M$ can be set equal to the interaction parameter $\Gamma$.[33] For the same reason the relaxation rate constant at $\gamma_{HS} = 1$ depends very little on the concentration, and therefore $k_{HL}^{0}\left(x,T\right) \approx k_{HL}^{0}\left(T\right)$. In the present simulation, we use the parameters found for the neat compound discussed in ref. 40,

namely, $\Delta H^0_{HL}$ = 395 K, $\Delta S^0_{HL}$ = 5 and $\Gamma = \Delta_M$ = 380 K. The values of the relaxation rate constant at $\gamma_{HS}$ = 1, $k^0_{HL}(T)$, at different temperatures as represented in Figure 7, have been obtained by numerically fitting the relaxation curves from Figures 5 and 6 for all systems which remain in $P\bar{3}$ under the given conditions. For the very dilute system with $x$ = 0.01, they just correspond to the rate constant at the given temperature. The values of $k^0_{HL}(T)$ for the tetrafluoroborate are slightly lower than those of the perchlorate analogue[47] shown for direct comparison in the same figure. For $x$ = 0.31, the sigmoidal character already becomes apparent and is accounted for by the above mean-field value of $\Gamma$.

Using the values of $k^0_{HL}(T)$ from Figure 7, interpolated and extrapolated for other temperatures of interest, and keeping the other parameter fixed, we calculate the expected kinetic curves in Figure 3, in which the temperature was scanned at 0.2 K/min starting from 10 K after the creation of different light-induced LS populations. The agreement with the experimental data is good, especially for low Fe concentrations and at the temperature where the relaxation sets in. However, for high iron(II) concentrations and high initial LS fractions deviations form mean-field behaviour are substantial. This is due to the fact that as soon as the kinetics of the crystallographic phase transition interferes with the kinetics of the intersystem crossing process, nucleation and growth phenomena create a domain structure, which modulates the intersystem crossing in a complex way.

Compared to the perchlorate analogue the above parameter set differs to some extent. $\Delta S^0_{HL}$ is within the approximations made the same and the value of $\Delta H^0_{HL}$ is only slightly larger. In contrast, the value of the interaction parameter $\Gamma$ is considerably larger. Within the mean-field approximation, $T_{1/2}$ for a potential spin transition in the dilute sample is estimated to be around 0 K, and as the hysteresis opens for higher concentrations, $T_c^{\downarrow}$ will be very close to 0 K too.

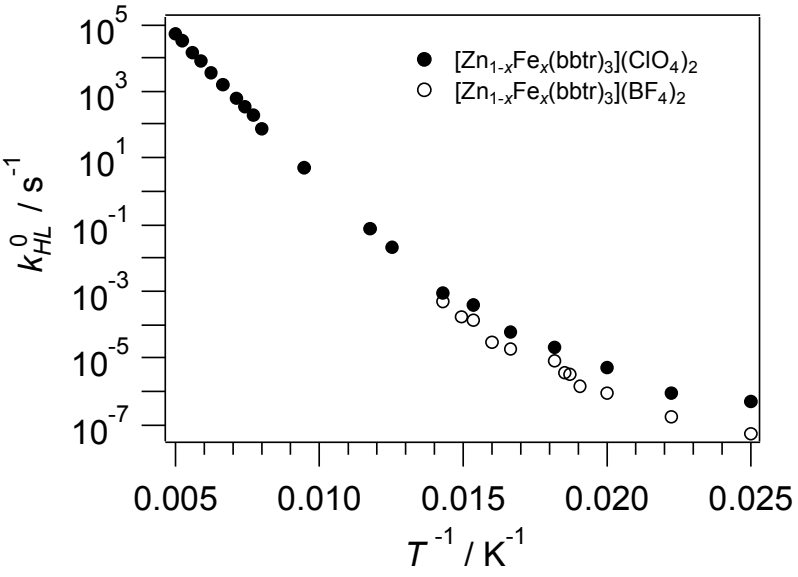


**Figure 7.** Dependence of $k^0_{HL}(T)$ on $T^{-1}$ for {[Zn$_{1-x}$Fe$_x$(bbtr)$_3$](BF$_4$)$_2$}$_\infty$ and {[Zn$_{1-x}$Fe$_x$(bbtr)$_3$](BF$_4$)$_2$}$_\infty$ together with those of the analogous perchlorate salt taken from ref. 47.

## 4. Conclusions

Variable temperature, optical single crystal spectroscopy making use of the very different extinction coefficients for spectroscopic transitions of different nature allow a detailed investigation of the light-induced spin transition and the ensuing relaxation processes in the solid solutions of {[Zn$_{1-x}$Fe$_x$(bbtr)$_3$](BF$_4$)$_2$}$_\infty$ over a wide concentration range, that is, from very dilute with $x$ = 0.01 to the neat iron(II) compound with $x$ = 1. In this system, strong cooperative effects of elastic origin play an important role, influencing both the thermal and photo-induced relaxation behaviour. For the highly diluted mixed-crystals of {[Zn$_{1-x}$Fe$_x$(bbtr)$_3$](BF$_4$)$_2$}$_\infty$, the cooperative effects are, of course, absent or weak, whereas in the concentrated or moderately concentrated mixed-crystals, they become strong enough to influence the photo-induced spin switching dynamics. Moreover, for the highly concentrated systems, the cooperative effects are so strong that they induce the observed macroscopic light-induced bistability. This bistable behaviour has been investigated as a function of iron(II) concentration and initial light-induced LS population, enabling us to established the limits of the light-induced bistability with critical

iron(II) concentration for the light-induced bistability is $x \approx 0.5$. The complex LS $\rightarrow$ HS relaxation behaviour as a function of temperature and time has also been discussed in terms of the interplay between the dynamics of the intersystem crossing process itself and the kinetics of the crystallographic phase transition. The experimental results were analysed quantitatively and reproduced the spin-state switching dynamics within the framework of the mean-field approximation satisfactorily within a given crystallographic phase. Finally, the spin-state switching behaviour in the mixed-crystals of $\{[Zn_{1-x}Fe_x(bbtr)_3](BF_4)_2\}_\infty$ and the influence of the cooperative effects presented here help us to understand the physics of structure-function correlations and constitute an important step towards possible potential applications in the field of photo-switching devices.

**Acknowledgements**

We thank D. Lovy and L. Devenoge of the University of Geneva for help with kinetic measurements. Financial support by the Swiss National Science Foundation (Grant No. 200020_137567), the Romanian National Research Council (Grants PCCE 9/2010 and TE 185/2010) is gratefully acknowledged. We also thank Philip Pattison for his help with the X-ray diffraction experiments and the Swiss Norwegian Beamline at the ESRF, Grenoble, for the provision of synchrotron beam time

**References**

1 Spin Crossover in Transition Metal Compounds I - III (P. Gütlich, H. A. Goodwin, eds), *Top. Curr. Chem. 233-235*, Springer, Heidelberg, **2004**.

2 A. Bousseksou, G. Molnár, L. Salmon, W. Nicolazzi, *Chem. Soc. Rev.* **2011**, *40*, 3313.

3 F. Prins, M. Monrabal-Capilla , E. A. Osorio , E. Coronado, H. S. J. van der Zant, *Adv. Mater.* **2011**, *23*, 1545.

4 J. Jeftic, A. Hauser, *J. Phys. Chem. B* **1997**, *101*, 10262.

5 P. Gütlich, V. Ksenofontov, A. B. Gaspar, *Coord. Chem. Rev.* **2005**, *249*, 1811.

6 A. Bousseksou, N. Negre, M. Goiran, L. Salmon, J-P. Tuchagues, M-L. Boillot, K. Boukheddaden, F. Varret, *Eur. Phys. J. B*, **2000**, *13*,451.

7 S. Bonhommeau, G. Molnár, M. Goiran, K. Boukheddaden, A. Bousseksou, *Phys. Rev. B* **2006**, *74*, 064424.

8 M. Ohba, K. Yoneda, G. Agusti, M. C. Munoz, A. B. Gaspar, J. A. Real, M. Yamasaki, H. Ando, Y. Nakao, S. Skaki, S. Kitagawa, *Angew. Chem., Int. Ed.* **2009**, *48*, 4767.

9 a) P. Gütlich, A. Hauser, H. Spiering, *Angew. Chem.* **1994**, *106*, 2971; b) A. Hauser, *Top. Curr. Chem.* 2004, 234, 155; (c) S. Decurtins, P. Gütlich, C. P. Köhler, H. Spiering, A. Hauser, *Chem. Phys. Lett.* **1984**, *139*, 1.

10 P. Gütlich, P. J. van Koningsbruggen, F. Renz, Struct. Bond. (Berlin, Germany) **2004**, *107*, 27.

11 a) A. Hauser, *Chem. Phys. Lett.* **1986**, *124*, 543, b) A. Hauser, *J. Chem. Phys.* **1991**, *94*, 2741.

12 a) I. Krivokapic, C. Enachescu, R. Bronisz, A. Hauser, *Chem. Phys. Lett.* **2008**, *455*, 192; b) I. Krivokapic, C. Enachescu, R. Bronisz, A. Hauser, *Inorg. Chim. Acta* **2008**, *361*, 3616.

13 a) E. A. Juban, A. L. Smeigh, J. E. Monat, J. K. McCusker, *Coord. Chem. Rev.* **2006**, *250*, 1783, b) N. Huse, H. Cho, K. Hong, L. Jamula, F. M. F. de Groot, T. K. Kim, J. K. McCusker, R. W. Schoenlein, *J. Phys. Chem. Lett.* **2011**, *2*, 880, c) M. Chergui, *Dalton Trans.* **2012**, *41*, 13022, Ch. Bressler, C. Milne, V.-T. Pham, A. ElNahhas, R. M. van der Veen, W. Gawelda, S. Johnson, P. Beaud, D. Grolimund, M. Kaiser, C. N. Borca, G. Ingold, R. Abela, M. Chergui, *Science* **2009**, *323*, 489

14 A. Marino, P. Chakraborty, M. Servol, M. Lorenc, E. Collet, A. Hauser, *Angew. Chem. Int. Ed.* **2014**, *53*, 3863.

15 P. Guionneau, M. Marchivie, G. Bravic, J.-F. Létard, D. Chasseau, *Top. Curr. Chem.* **2004**, *234*, 97.

16 J. Kusz, P. Gütlich, H. Spiering, Top. Curr. Chem. 2004, 234, 129.

17 (a) J. -P. Martin, J. Zarembowitch, A. Dworkin, J.G. Haasnoot, E. Codjovi, *Inorg. Chem.* **1994**, *33*, 2617; (b) J.-P. Martin, J. Zarembowitch, A. Bousseksou, A. Dworkin, J. G. Haasnoot, F. Varret, *Inorg. Chem.* **1994**, *33*, 6325.

18 J. Kusz, R. Bronisz, M. Zubko, G. Bednarek, *Chem. Eur. J.* **2011**, *17*, 6807.

19 a) J. Kusz, H. Spiering, P. Gütlich, *J. Appl. Cryst.* **2000**, *33*, 201; b) J. Kusz, D. Schollmeyer, H. Spiering, P. Gütlich, *J. Appl. Cryst.* **2005**, *38*, 528; c) H. Ayanagi, T. Tayagaki, K. Tanaka, *J. Phys. Chem. Sol.* **2004**, *65*, 1485; d) V. A. Money, J. Elhaik, I. R. Evans, M. A. Halcrow, J. A. K. Howard, *Dalton Trans.* **2004**, 65.

20 A. Hauser, Top. Curr. Chem. **2004**, *233*, 49.

21 A. Tissot, M.-L. Boillot, S. Pillet, E. Codjovi, K. Boukheddaden, L. M. L. Daku, *J. Phys. Chem. C*, **2010**, *114*, 21715.

20 Y. Hasegawa, K. Takahashi, S. Kume and H. Nishihara, *Chem. Comm.* **2011**, *47*, 6846.

23 D. Chernyshov, B. Vangdal, K. W. Törnroos, H.-B. Bürgi, *New J. Chem.* **2009**, *33*, 1277.

24 J. M. Holland, J. A. McAllister, Z. Lu, C. A. Kilner, M. Thornton-Pett, M. A. Halcrow, *Chem. Comm.* **2001**, 577.

25 K. W. Törnroos, M. Hostettler, D. Chernyshov, B. Vangdal, H. -B. Bürgi, *Chem. Eur. J.* **2006**, *12*, 6207.

26 D. Chernyshov, N. Klinduhov, K. W. Törnroos, M. Hostettler, B. Vangdal, H. -B. Bürgi, *Phys. Rev. B*, **2007**, *76*, 014406.

27 A. Hauser, J. Jeftic, H. Romstedt, R. Hinek, H. Spiering, *Coord. Chem. Rev.* **1999**, *190-192*, 471-491.

28 R. Jakobi, H. Spiering, L. Wiehl, E. Gmelin, P. Gütlich, *Inorg. Chem*. **1988**, *27*, 1823.

29 M. A. Halcrow, *Chem. Soc. Rev.* **2011**, *40*, 4119.

30 C.P. Slichter, H.G. Drickamer, *J. Chem. Phys.* **1972**, *56*, 2142.

31 F. Varret, K. Boukheddaden, E. Codjovi, C. Enachescu, J. Linares, *Top. Curr. Chem.* **2004**, *234*, 199.

32 S. I. Klokishner, M. A. Roman, O. S. Reu, *Inorg. Chem.* **2011**, *50*, 11394.

33 H. Spiering, *Top. Curr. Chem.* **2004**, *235*, 171.

34 J. -F. Létard, *Top. Curr. Chem.* **2004**, *235*, 221.

35 M. Matsuda, H. Tajima, patent no JP2009212164-A, **2009**.

36 R. Bronisz, *Inorg. Chem.* **2005**, *44*, 4463.

37 P. Chakraborty, R. Bronisz, C. Besnard, L. Guénée, P. Pattison, A. Hauser, *J. Am. Chem. Soc.* **2012**, *134*, 4049.

38 a) W. Morscheidt, J. Jeftic, E. Codjovi, J. Linares, A. Bousseksou, H. Constant-Machado, F. Varret, *Meas. Sci. Technol*. **1998**, *9*, 1311; b) L. Salmon, G. Molnár, S. Cobo, P. Oulié, M. Etienne, T. Mahfoud, P. Demont, A. Eguchi, H. Watanabe, K. Tanaka, A. Bousseksou, *New J. Chem*. **2009**, ***33***, 1283.

39 P. Chakraborty, C. Enachescu, C. Walder, R. Bronisz, A. Hauser, *Inorg. Chem.* **2012**, *51*, 9714.

40 P. Chakraborty, S. Pillet, E.-E. Benedeif, C. Enachescu, R. Bronisz, A. Hauser, *Chem. Eur. J.* **2013**, *19*, 11418.

41 (a) R. Hinek, H. Spiering, P. Gütlich, A. Hauser, *Chem. Eur. J.* **1996**, *2*, 1435; (b) *Chem. Eur. J.* **1996**, *2*, 1427; (c) P. Poganiuch, S. Decurtins, P. Gütlich, *J. Am. Chem. Soc.***1990**, *112*, 3270.

42 (a) H. Spiering, E. Meissner, H. Koppen, E.W. Müller, P. Gütlich, *Chem. Phys.* **1982**, *68*, 65; (b) C. P. Köhler, R. Jakobi, E. Meissner, L. Wiehl, H. Spiering, P. Gütlich, *J. Phys. Chem. Solids* **1990**, *51*, 239.

43 S. Cobo, D. Ostrovski, S. Bonhommeau, L. Vendier, G. Molnár, L. Salmon, K. Tanaka, A. Bousseksou, *J. Am. Chem. Soc.* **2008**, *130*, 9019.

44 S. Bonhommeau, G. Molnár, S. Cobo, D. Ostrovski, A. Bousseksou, *Polyhedron* **2009**, *28*, 1610.

45 N. O. Moussa, D. Ostrovski, V. Martinez Garcia, G. Molnár, K. Tanaka, A. B. Gaspar, J. A. Real, A. Bousseksou, *Chem. Phys. Lett.* **2009**, *477*, 156.

46 G. Galle, J. Degert, C. Mauriac, C. Etrillard, J. -F. Létard, E. Freysz, *Chem. Phys. Lett.* **2010**, *500*, 18.

47 I. Krivokapic, P. Chakraborty, R. Bronisz, C. Enachescu, A. Hauser, *Angew. Chemie* **2010**, *122*, 8688; *Angew. Chem. Int. Ed.* **2010,** *49*, 8509.

**Graphical content entry**

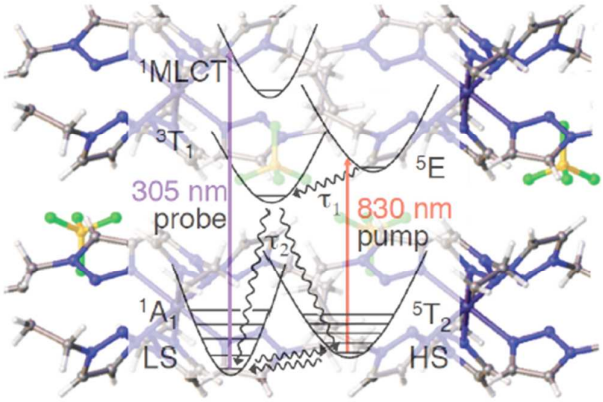


In the iron(II) spin-crossover polymer, strong cooperative interactions result in a light-induced bistability between the high-spin and the low-spin state.